# High Entropy Sulfide Nanoparticles as Lithium Polysulfide Redox Catalysts

M. J. Theibault<sup>a</sup>, Connor R. McCormick<sup>b</sup>, Shuangyan Lang<sup>a</sup>, Raymond E. Schaak<sup>b\*</sup>, Hèctor D. Abru-ña<sup>a\*</sup>

<sup>a</sup>Department of Chemistry and Chemical Biology, Cornell University, 245 Feeney Way, Ithaca, New York 14850, United States.

<sup>b</sup>Department of Chemistry, Department of Chemical Engineering, and Materials Research Institute, 104 Chemistry Building, The Pennsylvania State University, University Park, Pennsylvania 16802, United States.

KEYWORDS. "lithium sulfur" "electrochemical catalysis" "high entropy materials" "cocktail effect" "battery catalysis" "polysulfide shuttle" "high entropy sulfide"

**ABSTRACT:** The polysulfide shuttle contributes to capacity fade in lithium-sulfur batteries, which limits their practical utilization. Materials that catalyze the complex redox reactions responsible for the polysulfide shuttle are emerging, but foundational knowledge that enables catalyst development remains limited, with only a small number of catalysts identified. Here, we employ a rigorous electrochemical approach to show quantitatively that the lithium polysulfide redox reaction is catalyzed by nanoparticles of a high entropy sulfide material,  $Z_{10.30}C_{00.31}C_{00.19}I_{10.13}G_{30.06}S$ . When 2% by weight of the high entropy sulfide is added to the lithium sulfur cathode composite, the capacity and coulombic efficiency of the resulting battery are improved at both moderate (0.2 C) and high (1 C) charge/discharge rates. Surface analysis of the high entropy sulfide nanoparticles using X-ray photoelectron spectroscopy provides important insights into how the material evolves during the cycling process. The  $Z_{10.30}C_{00.31}C_{00.19}I_{10.13}G_{30.06}S$  nanoparticle catalyst outperformed the constituent metal sulfides, pointing to the role that the high-entropy "cocktail effect" can play in the development of advanced electrocatalytic materials for improved lithium sulfur battery performance.

INTRODUCTION. The polysulfide shuttle is the process by which liquid-phase polysulfides diffuse from the cathode to the lithium metal anode in lithium sulfur batteries. This polysulfide shuttle causes extensive capacity fade and is one of the main barriers to commercialization of lithium sulfur batteries, despite having high earth abundance, low cost, and a theoretical capacity that is nearly ten times higher than that of existing commercial lithium ion battery materials (1675 mAh g-1).1-4 Catalysts have been developed to overcome the polysulfide shuttle, particularly the liquidsolid transition step of intermediate chain polysulfides to insoluble short chain polysulfides. For example, metal sulfides such as NiS, CoS<sub>2</sub>, and TiS<sub>2</sub><sup>5-10</sup> have been added to lithium sulfur batteries to catalyze the redox reactions that contribute to the polysulfide shuttle, thereby improving initial capacity and capacity retention in the batteries. However, the development of catalytic materials for lithium sulfur batteries has to date been limited.

High entropy materials, which typically contain five or more elements randomly distributed throughout a crystal lattice, 11-13 have unique catalytic properties that are directly relevant to overcoming performance limitations due to the polysulfide shuttle. The large number of homogenously mixed and distributed metals in a high entropy material produces a "cocktail effect", which is the colloquial term that describes the resulting synergistic properties that arise

from the interactions among the constituent elements. This cocktail effect results in chemically and electronically diverse adsorption sites for catalyzing complex chemical reactions<sup>14-18</sup>, such as the lithium polysulfide redox reaction that involves a large number of intermediates in equilibrium with one another. Nanostructured high entropy materials can further enhance catalytic performance by providing a high volumetric and gravimetric density of surface-exposed active sites<sup>11,15</sup>. Co-doped ZnS and CoS are known catalytic materials for lithium sulfur batteries and Cu-based additives in Li-S batteries have been studied. 5,6,8-10 These considerations motivate the incorporation of Zn, Co, and Cu into a sulfide material, along with additional elements (In, Ga) to balance charge. Accordingly, here we demonstrate that nanoparticles of a high entropy sulfide material,  $Zn_{0.30}Co_{0.31}Cu_{0.19}In_{0.13}Ga_{0.06}S$ , significantly increase the rate of the polysulfide redox reaction and therefore minimize the detrimental effects of the polysulfide redox shuttle for improved lithium sulfur batteries. The constituent metal sulfides do not catalyze the polysulfide redox reaction, which points to the unique role of the high entropy sulfide. Additionally, when 2% of  $Zn_{0.30}Co_{0.31}Cu_{0.19}In_{0.13}Ga_{0.06}S$  was included as an additive in a lithium sulfur battery, the initial capacity improved significantly when compared to non-catalyzed batteries.

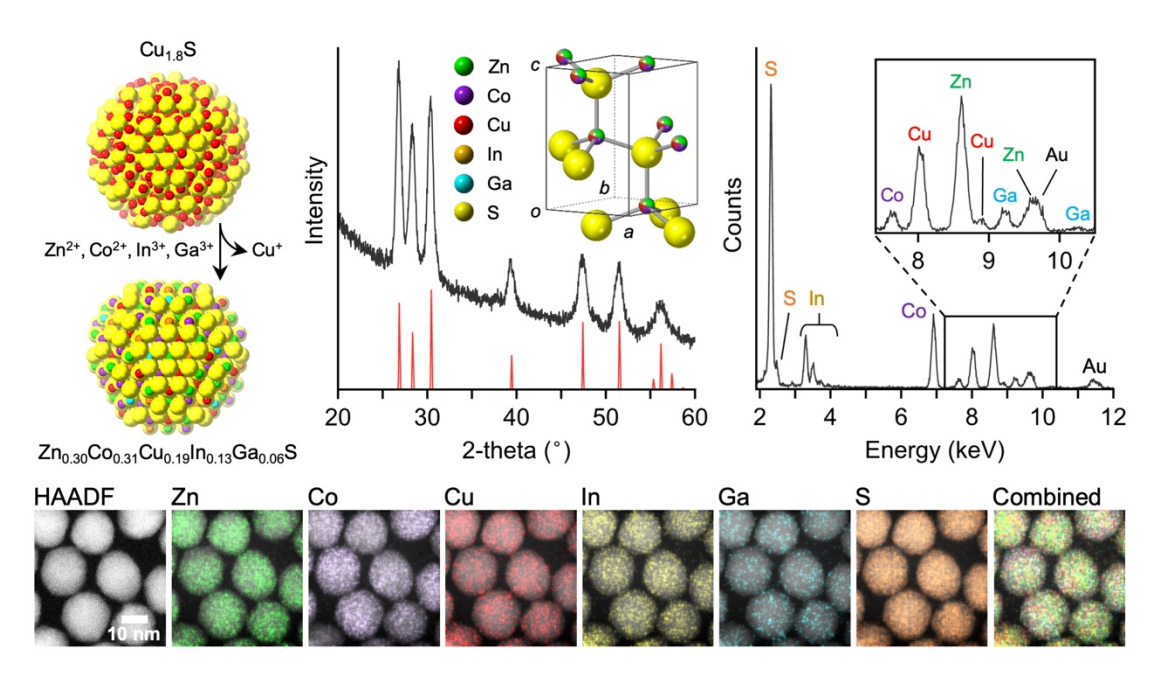


**Figure 1.** (a) Schematic showing the synthesis of  $Z_{10.30}C_{00.31}C_{00.19}I_{10.13}G_{30.06}S$  nanoparticles by simultaneous multi-cation exchange of  $Z_{10.8}S$  nanoparticles. (b) Powder XRD pattern of the  $Z_{10.30}C_{00.31}C_{00.19}I_{10.13}G_{30.06}S$  nanoparticles (black) with a simulated wurtzite pattern (red) shown for comparison. The wurtzite unit cell (a = 3.83 Å, c = 6.29 Å) is shown in the inset along with depictions of the crystal structures of roxbyite  $Z_{10.8}S$  and the high entropy sulfide with the cations randomly distributed among the cation sites of the wurtzite crystal structure. (c) EDS spectrum of the  $Z_{10.30}C_{00.31}C_{10.19}I_{10.13}G_{30.06}S$  nanoparticles. The Au signal originates from the Au TEM grids. (d) HAADF-STEM image and corresponding STEM-EDS elemental maps ( $Z_{10.19}I_{10.13}G_{30.06}S$  nanoparticles, along with a combined image.

RESULTS AND DISCUSSION. High Entropy Sulfide Nanoparticle Synthesis

Nanoparticles of the high entropy sulfide  $Zn_{0.30}Co_{0.31}Cu_{0.19}In_{0.13}Ga_{0.06}S$  were synthesized using a simultaneous multi-cation partial exchange of the Cu<sup>+</sup> cations in copper sulfide (Cu<sub>1.8</sub>S) with Zn<sup>2+</sup>, Co<sup>2+</sup>, In<sup>3+</sup>, and Ga<sup>3+</sup>, as shown schematically in Figure 1a.11 The cation exchange reaction was carried out by rapidly injecting a solution of spherical nanoparticles of roxbyite Cu<sub>1.8</sub>S (Figure S1) suspended in trioctylphosphine into a solution containing ZnCl<sub>2</sub>, CoCl<sub>2</sub>, InCl<sub>3</sub>, and GaCl<sub>3</sub>, along with oleylamine, octadecene, and benzyl ether, and heating to 140 °C for 30 min. 19 Additional experimental details are included in the Supporting Information.

The powder X-ray diffraction (XRD) pattern of the isolated high entropy sulfide nanoparticles matches well to a single wurtzite phase having lattice parameters of a = 3.83Å and c = 6.29 Å (Figure 1b). These lattice parameters are intermediate between those of the smallest (CoS: a = 3.73 Å, c = 6.16 Å) and largest (CuInS<sub>2</sub>: a = 3.91 Å, c = 6.43 Å) end members. The lattice parameters match well with a weighted average of all constituent metal sulfides (ZnS, CoS, CuInS<sub>2</sub>, CuGaS<sub>2</sub>), based on the composition determined from the EDS spectrum in Figure 1c, which shows that all elements are present throughout a large ensemble of particles. 11 The scanning transmission electron microscopy (STEM) data in Figure 1d indicated that the product consisted of 18 ± 2 nm (n=150) spherical nanoparticles. STEM data coupled with EDS mapping (STEM-EDS) indicated that the signals for Zn, Co, Cu, In, Ga, and S overlap uniformly within individual particles, which is consistent with the homogeneous mixing and distribution expected for a high entropy material (Figure 1d). Collectively, the characterization data validate the high-yield formation of  $Zn_{0.30}Co_{0.31}Cu_{0.19}In_{0.13}Ga_{0.06}S$  nanoparticles.

Impact of the High Entropy Sulfide on Reaction Kinetics

By applying a slurry of carbon, polyvinylidene fluoride (PVDF), and the high entropy sulfide nanoparticles to a glassy carbon (GC) electrode and running electrochemical experiments with the electrode immersed in a 1 mmol Li<sub>2</sub>S<sub>6</sub> solution, it is possible to mimic key aspects of the battery charging and discharging process. Varying the rotation rate for RDE experiments allows for direct measurement of the current that is based only on the kinetics of the reaction. For CV measurements of a carbon slurry modified electrode (Figure 2a), the peak corresponding to oxidation of Li<sub>2</sub>S<sub>6</sub> to S<sub>8</sub> was located at approximately -0.717 V, with its re-reduction at -0.977 V, with  $i_{pk}$  for the oxidation of 0.08 mA. The peak corresponding to reduction of Li<sub>2</sub>S<sub>6</sub> to Li<sub>2</sub>S<sub>m</sub> (m≤2) was located at approximately -1.18 V, with its re-oxidation at -1.045 V, and with ipk of -0.045 mA. The oxidation/reduction process of Li<sub>2</sub>S<sub>6</sub> to S<sub>8</sub> and back had a ΔE<sub>pk</sub> of 260 mV, indicating a quasireversible reaction, and the process of Li<sub>2</sub>S<sub>6</sub> to  $\text{Li}_2S_n$  (n≤6) had a  $\Delta E_{pk}$  of 140 mV. Using a rotating disc electrode (RDE) (Figure 2b), the kinetic regime for the oxidation reaction had E<sub>onset</sub> at -0.890 V and reached the mass transport limit at approximately -0.585 V. For the reduction reaction, E<sub>onset</sub> was -1.070 V, and the mass transport limit was reached at -1.225 V. The RDE results therefore indicated that addition of the high entropy

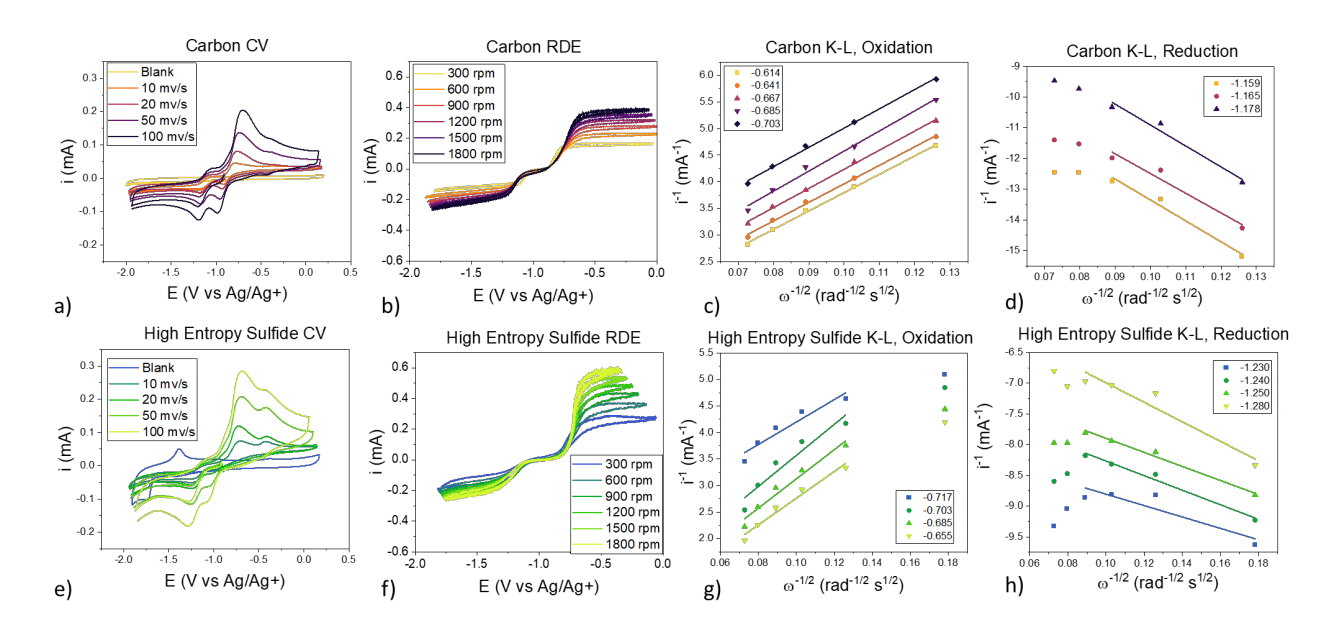


Figure 2. All plots were obtained in 0.1 M LiTFSI DOL/DME electrolyte with 1 mmol Li<sub>2</sub>S<sub>6</sub>. RDEs were taken at 20 mV/s. a) CV of Li<sub>2</sub>S<sub>6</sub> with a carbon slurry coated glassy carbon electrode taken at multiple scan rates. The blank solution has no Li<sub>2</sub>S<sub>6</sub>. B) RDE taken at multiple rotation rates under the same conditions. C) Koutecky-Levich plot for the oxidation reaction of Li<sub>2</sub>S<sub>6</sub> with a carbon-modified electrode. D) Koutecky-Levich plot of the reduction reaction of Li<sub>2</sub>S<sub>6</sub>. E) CV of Li<sub>2</sub>S<sub>6</sub> with a glassy carbon electrode coated with a high entropy sulfide slurry taken at multiple scan rates. The blank solution has no Li<sub>2</sub>S<sub>6</sub>. F) RDE taken at multiple rotation rates under the same conditions. G) Koutecky-Levich plot for the oxidation reaction of Li<sub>2</sub>S<sub>6</sub> on an electrode coated with a high entropy sulfide slurry. H) Koutecky-Levich plot of the reduction reaction of Li<sub>2</sub>S<sub>6</sub>.

sulfide nanoparticles to a polysulfide solution improved the kinetics of the polysulfide redox reaction, as compared to a plain carbon modified electrode without the high entropy nanoparticle catalyst.

Koutecky-Levich (K-L) analysis, which extracts the kinetic current of a reaction, provides additional insights into the reaction kinetics. Theoretically, K-L analysis is valid only for simple one electron transfer processes. In practice, so long as the kinetic values are not taken as the actual, specific rate, but are instead used only to compare the rates of the same reaction under different conditions, it is valuable for analysis of catalysts. 20-25 K-L plots for the oxidation showed non-coupled electron transfer kinetics over theentire kinetic potential regime (Figure 2c). However, for the reduction (Figure 2d), a change in the electrochemical behavior emerges at high rotation rates (1500 and 1800 rpm), which we attribute to a short-lived intermediate that does not have enough time to react when the rotation rate is too high. 20,24,25

As a comparison, a CV run with a slurry film containing 4 mg of the high entropy sulfide and 1 mg of carbon, and no polysulfide in solution, showed small peaks at -1.39 V and -1.750 V (Figure 2e). These peaks are well separated from the polysulfide peaks, which for the scan at 20 mV/s occur at -0.735 V (Li<sub>2</sub>S<sub>6</sub> to S<sub>8</sub>) and -1.015 V (S<sub>8</sub> to Li<sub>2</sub>S<sub>6</sub>) with an i<sub>pk</sub> of 0.12 mA, then -1.230 V (Li<sub>2</sub>S<sub>6</sub> to Li<sub>2</sub>S<sub>n (n<6)</sub>) and -1.090 V (Li<sub>2</sub>S<sub>n (n<6)</sub> to Li<sub>2</sub>S<sub>6</sub>) with an i<sub>pk</sub> of -0.068 mA. The difference

in potential between the oxidation and reduction peaks  $(\Delta E_{pk})$  for the conversion of  $Li_2S_6$  to  $S_8$  and back with a slurry modified with the high entropy sulfide is 280 mV, and  $\Delta E_{pk}$  for the reduction of  $Li_2S_6$  to  $Li_2S_n$  (n<6) and back is 140 mV. This value is improved compared to the carbon slurry without the high entropy sulfide, as it shows greater reaction reversibility. The RDE (Figure 2f) plots at all rotation rates had an  $E_{onset}$  of -0.850 V for the oxidation and reached mass transport limit at -0.630 V. For the reduction,  $E_{onset}$  was -1.065 V, and the mass transport limit was reached at -1.175 V. The overpotential for both of these was also improved when compared to those of carbon. Peak currents,  $\Delta E_{pk}$ , kinetic current, and rate constant for the carbon and high entropy sulfide slurry reactions are tabulated in Table 1.

Table 1. Peak potentials, peak currents, kinetic currents, and rate constants for the oxidation and reduction of Li<sub>2</sub>S<sub>6</sub>, on carbon and high entropy sulfide modified electrodes, respectively.

	Carbon	High Entropy Sulfide	
$\Delta E_{pk,ox}$ (mV)	260	280	
ΔE <sub>pk,red</sub> (mV)	140	140	
i <sub>pk,ox</sub> (mA)	0.08	0.12	
i <sub>pk,red</sub> (mA)	-0.045	-0.068	
i <sup>0</sup> ox (A)	2.9x10 <sup>-5</sup>	1.40x10 <sup>-4</sup>	
k <sup>0</sup> ox (cm <sup>-1</sup> )	4.3x10 <sup>-4</sup>	2.06x10 <sup>-3</sup>	
i <sup>0</sup> red (A)	2.2x10 <sup>-6</sup>	2.4x10 <sup>-5</sup>	
k <sup>0</sup> red (cm <sup>-1</sup> )	2.6x10 <sup>-5</sup>	2.8x10 <sup>-4</sup>	

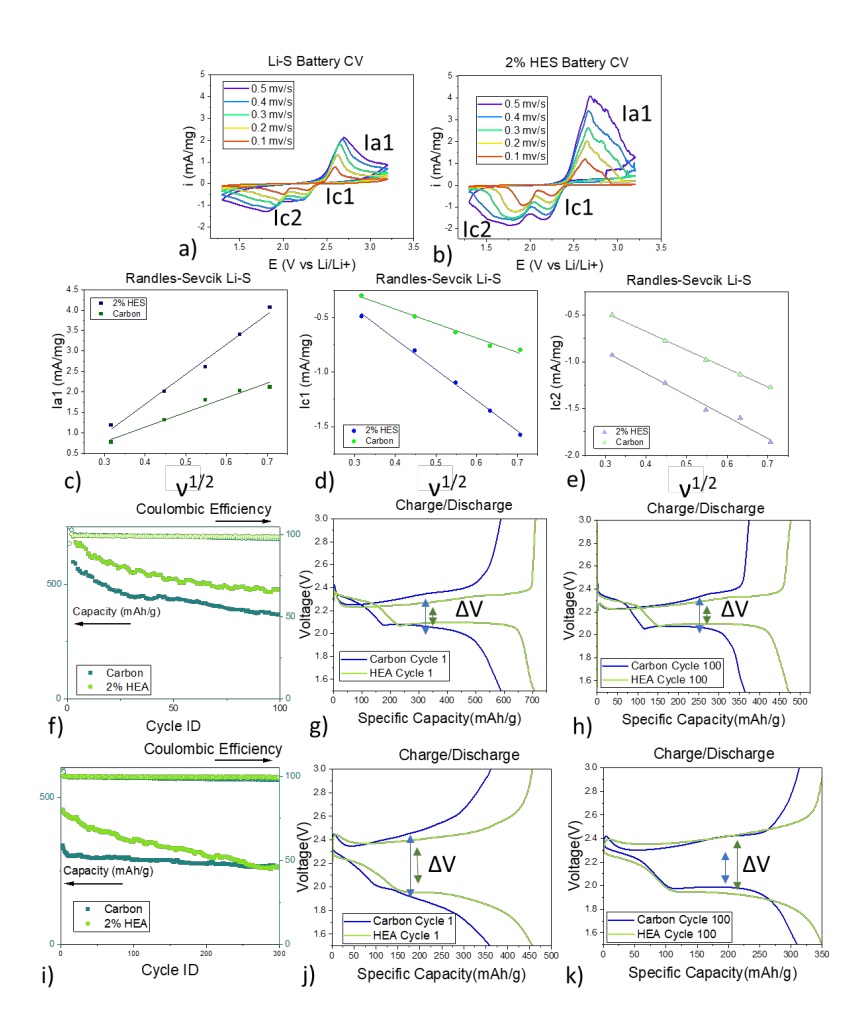


**Figure 3.** a) Battery CVs taken at multiple scan rates for a non-catalyzed Li-S battery. b) Battery CVs taken at multiple scan rates for a Li-S battery with 2% of the high entropy sulfide added. c,d,e) Randles-Sevcik plots of peak current vs the square root of the scan rate for the anodic and two cathodic redox peaks. f,i) Capacity retention of catalyzed and non-catalyzed batteries at 0.2 C and 1 C respectively, as well as coulombic efficiency. g,j) Charging and discharging capacity, at 0.2 C and 1 C respectively for catalyzed and non-catalyzed batteries during the first cycle, with overpotential indicated. h,k) Charging and discharging capacity, at 0.2 C and 1 C respectively for catalyzed and non-catalyzed batteries during the 100th cycle, with overpotential indicated.

Over the range of 600-1800 rpm, the oxidation kinetic regime appeared well-behaved, i.e., linear across the spread of potentials and rotation rates, by Koutecky-Levich analysis (Figure 2g). For the reduction (Figure 2h), however, the behavior was more complex. At low rotation rates the K-L plots had the expected linear form, but at high rotation rates the behavior seemed dependent on where in the kinetic regime the currents were sampled. At smaller overpotentials as compared to Eonset, the slope of the K-L plots changed from a positive value to a negative value at higher rotation rates. At higher overpotentials, which are closer to the mass transport limited regime, the steepness of the slope by K-L analysis changed at high rotation rates, though the sign did not change. When both carbon and the high entropy sulfide are compared, the high entropy sulfide has much improved kinetics, as shown by the i<sup>0</sup> and k<sup>0</sup> calculated from the K-L plots. It should be noted that comparing the reduction reaction for the high entropy sulfide modified slurry and the carbon slurry is difficult, as the shapes of the plots for the reduction reactions are different. In RDE measurements, the high entropy sulfide slurry exhibited a shift to slightly higher overpotentials from  $E_{\rm onset}$  as the rotation rate increased, while the carbon slurry did not. Nevertheless, we can still point to evidence of catalysis from other factors including the improved kinetic current of the oxidation reaction in RDE measurements, the enhanced peak currents in CV, and the decrease between  $E_{\rm onset}$  and  $E_{\rm mass\ transport}$  for both the oxidation and reduction reactions.

As mentioned earlier, high entropy materials often exhibit a catalytic "cocktail effect," whereby the large number of randomly mixed metals interact synergistically to produce catalysts having performance metrics that are improved relative to any constituent material or their weighted average.  $^{26,27}$  To compare the high entropy sulfide,  $Z_{10,30}Co_{0.31}Cu_{0.19}In_{0.13}Ga_{0.06}S$ , with each of its constituent metal sulfides, we ran RDE measurements of ZnS, CoS<sub>x</sub>,  $Cu_{1.8}S$ ,  $CuInS_2$ , and  $CuGaS_2$  nanoparticles of comparable

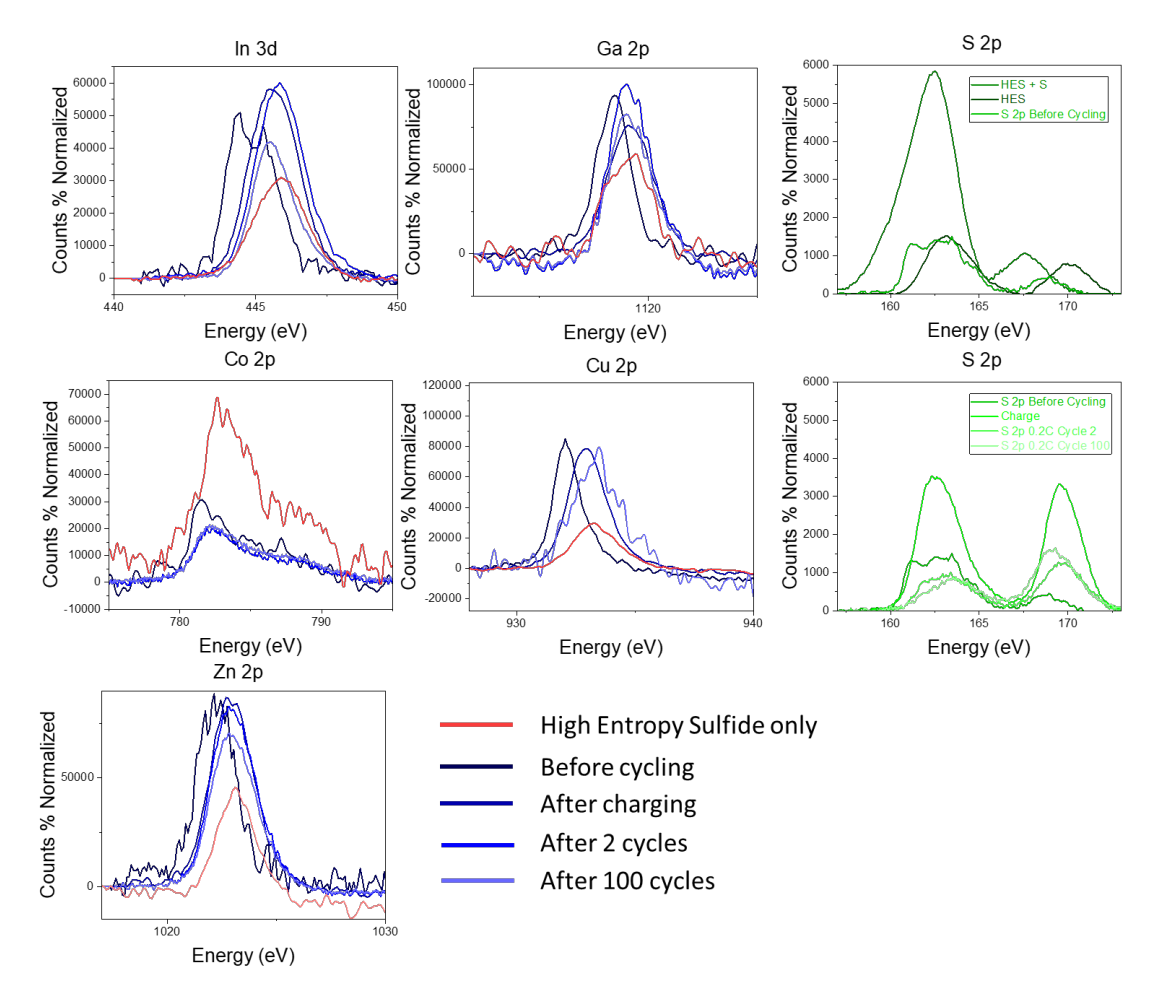


**Figure 4.** Binding Energies measured via XPS for sulfur and metal centers at different points in the battery cycling process. XPS data for In, Ga, Co, Cu, and Zn both in the pure high entropy sulfide and as a part of a cathode slurry at different points in the cycling process. XPS data for sulfur in the pure high entropy sulfide, in the high entropy sulfide with  $S_8$  added, and as part of a cathode slurry at different points in the cycling process.

sizes, size distributions, and morphologies (Figure S3). On the basis of the measured kinetic currents, the positions of those currents relative to  $E_{onset}$ , and values of  $i^0$ , none of the constituent metal sulfides exhibited higher performance than the high entropy sulfide for both the oxidation and the reduction (Table S2). An in-depth discussion of the components is included in the SI.

The main conclusion of these experiments, along with those reported above, is validation of the "cocktail effect," or synergistic interactions among the randomized elements, for this high entropy sulfide in its ability to function as a polysulfide redox catalyst. Though two components appear to catalyze the reduction reaction (GuGaS2 and CuInS2), none of them appear to catalyze the oxidation, while the HES shows much improved oxidation kinetics. The superior catalytic properties of the high entropy sulfide for polysulfide redox are therefore considered to arise from synergistic interactions. The question then becomes what would be the impact of a high entropy material whose constituent parts are all known lithium polysulfide redox catalysts, i.e., CoS and MoS<sub>2</sub>, and if the synergistic effects of these known catalysts could combine for even better kinetic and battery performance.

## **Battery Testing**

Given the improved catalytic currents, we tested CVs of batteries made without any catalyst and with 2% of the high entropy sulfide added to the electrode slurry (Figure 3a,b). When the peak current of these batteries at different scan rates was plotted versus the square root of the scan rate, for both the anodic and cathodic peaks, the slopes of the Randles-Sevcik plots were greater for the batteries that included the high entropy sulfide (Figure 3c,d,e). These results indicate improved lithium-ion diffusion in the batteries containing high entropy sulfide nanoparticles, and since faster reaction rates would drive improved lithium-ion diffusion, the CVs of batteries and the kinetic RDE data are consistent with one another.

Battery cycling tests at 0.2 C showed that batteries constructed with 2% high entropy sulfide nanoparticles exhibited improved capacities, as well as improved capacity retention. The initial capacity for a non-catalyzed/carbon battery was 595 mAh/g, versus 706 mAh/g for the catalyzed/high entropy sulfide battery. Additionally, after 100 cycles, the non-catalyzed batteries showed a capacity of 369 mAh/g (62% retention) versus 480 mAh/g (68% retention) for the catalyzed batteries. The overpotential for charging

and discharging was also improved for the catalyzed batteries, both for the first cycle (173 mV for the high entropy sulfide battery vs 240 mV for the carbon battery) and after 100 cycles (175 mV HES vs 220 mV carbon), indicating stability of the catalyst for at least up to 100 cycles (Figure 3f,g,h).

At 1C, the catalyzed batteries showed an improved initial capacity (456 mAh/g) as compared to the non-catalyzed batteries (335 mAh/g). However, at these faster charging rates, the capacity retention for the catalyzed battery was much lower at 57% compared to the non-catalyzed batteries, which was 71%, after 300 cycles (Figure 3i). The improved initial capacity provides some evidence for catalysis within the battery, as the conversion-type reaction is responsible for the battery capacity. This shows that at higher charging rates, there is higher utilization in the battery containing high entropy sulfide nanoparticles, which provides evidence for the reactions being catalyzed by the high entropy sulfide. For the first cycle, the catalyzed battery had a smaller charging/discharging overpotential as compared to the non-catalyzed battery (463 mV vs 645 mV). However, at the 100th cycle, the non-catalyzed battery had a lower overpotential for charging/discharging (443 mV for the catalyzed battery vs 403 mV for the non-catalyzed battery) (Figure 3j,k), perhaps indicating that the catalyst begins to fail at this point. The lower capacity retention of the catalyzed batteries at higher rates could indicate that the volumetric expansion of sulfur during cycling causes it to become detached from the current collector, therefore leading to lower sulfur utilization. Using a simple physical mixing procedure, improvements in initial capacity and capacity retention are observed, illustrating the performance advantage of adding high entropy sulfide nanoparticles to a Li-S battery system.

Surface Characterization by X-ray Photoelectron Spectroscopy

X-ray photoelectron spectroscopy (XPS) was employed to characterize the chemical bonding environment surrounding the metal centers in the high entropy sulfide to understand its role during the charging and discharging processes (Figure 4). XPS spectra were acquired for the high entropy sulfide initially (as-synthesized), at a concentration of 10% in a slurry and on a carbon/aluminum current collector before cycling, and at a concentration of 10% in a battery after being discharged at 0.05 C, after being charged/discharged at 0.05 C for 2 cycles, and after being charged/discharged at 0.2 C for 100 cycles. XPS data for the pure high entropy sulfide nanoparticles indicate that the metal centers are all at a higher oxidation state than they would be in their native sulfides (Table S3) and that incorporating the high entropy sulfide into a carbon slurry causes the binding energies to decrease, indicating that sulfur reduces the high entropy sulfide when the two are mixed. The metal centers all become oxidized again as cycling begins.

Additional insights are provided by XPS data for sulfur. For the high entropy sulfide nanoparticles, there are two major sulfur peaks. The first, which is a broad peak around 163 eV, is at a binding energy that is consistent with a sulfur-metal bond, as expected given the many metal-sulfur bonds in the material. The second, which is a slightly smaller peak at 170 eV, likely corresponds to a metal sulfate that suggests surface oxide formation. When  $S_{\mbox{\tiny B}}$  is mixed in

with the high entropy sulfide, these two peaks shift to a lower binding energy and the lower energy peak, which corresponds to the location of the sulfur in  $S_8$ , becomes much higher in intensity. As with the metal centers, the sulfur 2p peak in the slurry shifts to a lower binding energy as compared to the pure high entropy sulfide.

The sulfur XPS data indicate that after the discharging step, both the metal sulfate and metal sulfide peaks increase in intensity, even when normalized to atomic percent; the former likely from TFSI anions depositing on the surface. Additionally, moving from the precycle XPS data to the XPS data after 100 cycles, the metal sulfate peaks increase in intensity while the metal sulfide peaks remain approximately the same. This observation suggests that more of the sulfur in the composite is in the form of metal sulfate, rather than metal sulfide, as cycling continues and that the ratio of metal-sulfate to metal-sulfide increases. This change in ratio is not caused by the formation of Li<sub>2</sub>S, as those peaks would appear around 163 eV. To understand the origin of this behavior, we must consider the atomic percentages of all of the metal centers, as well as sulfur, at each step in which XPS data were collected (Table 2).

**Table 2.** Atomic percentages for In, Cu, Co, Zn, Ga, and S for various XPS runs.

Peak	At %	At %	At %	At %
	Before Cycling	Precycle	100 Cycles 0.2 C	100 Cycles 1 C
In 3d	3.5	15.7	16.4	19.7
Cu 2p	5.8	0.56	0.7	0.45
Co 2p	1.9	8.5	8.5	3.5
Zn 2p	1.9	6.4	7.5	8.4
Ga 2p	1.0	1.6	1.9	1.5
S 2p	85.9	67.2	64.9	66.5

Compared to the bulk percentages of the metal centers, when normalized to the percentage of sulfur, the surface concentration of indium is 12%, copper is 8.2%, cobalt is 1.5%, and zinc is 2.9%. The amount of gallium on the surface was below detection limits. The surface appears to contain predominantly sulfur, and interestingly, while cobalt and zinc have a higher concentration in the bulk, indium and copper have a higher concentration on the surface. The ratios of indium and copper, and zinc and cobalt, appear to be constant with each other.

The atomic percentages of the metal centers and sulfur were analyzed before the battery was cycled, after the 0.05 C precycle, and then after 100 cycles both at 0.2 C and 1 C. The atomic percentage of sulfur decreased after 100 cycles from 86% to about 65%, which is expected, as polysulfide dissolution is one of the main failure mechanisms (capacity fade) in lithium sulfur batteries. This dissolution of sulfur would be expected to correspond to a concomitant increase in the relative atomic percentage of the metal centers, as is indeed observed for indium, zinc, cobalt, and gallium. However, the atomic percentage of copper decreased by an

order of magnitude after 100 cycles. We postulate that copper is leaching from the high entropy sulfide by reacting with the anionic TFSI that deposits upon cycling. Previous Li-S Raman experiments indicate that during the discharging process, TFSI- will deposit at the electrolyte/lithium interface, indicating its participation in cycling.<sup>28</sup> Assuming it deposits on the cathode surface as well, this system requires further evaluation to determine the precise mechanism of loss of copper. Though somewhat speculative on our part, we posit that the TFSI could be depositing onto the cathode surface, possibly due to interactions with the copper cations there, and is then reacting with those copper cations to form CuTFSI. This species is similarly soluble in the electrolyte, and therefore the copper can leach out as an ionic species. Interestingly, the copper 2p peak after 100 cycles is also the only peak among all metal centers that is present at a higher binding energy than the pure high entropy sulfide, 935.5 eV, and this binding energy is that of the Cu (II) peak in CuSO<sub>4</sub>. All of this combined evidence suggests that copper is likely leaching in the form of CuTFSI during cycling. Much like the evidence of the cocktail effect, this indicates that stabilizing the cations, so they do not leach out, could prolong catalyst life, improving capacity and capacity retention beyond even the improvements made in this work. This is a very promising indication for future high entropy sulfide catalytic research in the field of lithium sulfur batteries.

In addition to XPS analysis, particles were imaged after being used in the battery. TEM images of particles taken after 20 cycles are shown in Figures S7 and S8. These images show that the particles appear smaller after catalysis, as they changed from monodisperse 18-nm spheres to poly-disperse nanoparticles with irregular shapes and average diameters of < 10 nm. Based on EDS analysis, all five elements are still present in the particles. However, the amount of Cu present in the particles after catalysis is less than before catalysis (Figures S7, Figure S8, and Table S4). Some particles are still crystalline after catalysis (Figure S8), but most particles have lower crystallinity, which is consistent with the leaching of Cu and the decrease in size that were observed as a result of cycling.

CONCLUSIONS. Nanoparticles of the high entropy sulfide  $Zn_{0.30}Co_{0.31}Cu_{0.19}In_{0.13}Ga_{0.06}S$ , synthesized through simultaneous multi-cation exchange of Cu<sub>1.8</sub>S nanoparticles, have been shown to catalyze the lithium polysulfide redox reactions that lead to the polysulfide shuttle that has detrimental impacts on lithium-sulfur battery performance. The rate constant for the catalyzed redox reaction was higher than that of the non-catalyzed reaction, and the kinetics were improved when using the high entropy sulfide catalyst as compared to its constituent metal sulfides, which points to the importance of the high entropy "cocktail effect" in achieving the improved kinetics. Upon adding only 2% by weight of the high entropy sulfide nanoparticles to the battery slurry, the battery capacity was improved both at typical charging rates and at high charging rates. An ex-situ XPS study of the high entropy sulfide catalyst, as synthesized and at multiple points in the charging/discharging process, indicated that in the battery, the metal centers in the high entropy sulfide are more reduced than in their parent compounds, while they progressively shift to higher oxidation states upon cycling. Additionally, copper appears to leach from the battery as it is cycled, indicating that in a future work ensuring no cations leach will likely improve battery performance even beyond what was observed in this work.

This study demonstrates that high entropy sulfides can catalyze the lithium polysulfide redox reactions to improve lithium sulfur battery performance. It also provides a fundamental understanding of the chemical changes that occur as the high entropy sulfide catalyst evolves during the charging/discharging processes. These insights provide a foundation for understanding how high entropy materials can be incorporated into electrochemical energy storage systems. For future work, we anticipate that a high entropy material where each component is a known lithium sulfur redox catalyst will show even greater improvements in battery performance. The discovery of additional high entropy composition, perhaps through emerging combinatorial libraries of high entropy and polyelemental sulfide materials <sup>29-31</sup>, could further expand the field of lithium sulfur electrocatalysts.

### ASSOCIATED CONTENT

Materials synthesis (Table S1, Figure S1), electrochemical experimental procedure, additional electrochemical experiments (Figure S2-8, Table S2-4) is supplied as Supporting Information. This material is available free of charge via the Internet at http://pubs.acs.org

#### **AUTHOR INFORMATION**

### Corresponding Author

Professor Héctor D. Abruña

Department of Chemistry and Chemical Biology, Cornell University, 245 Feeney Way, Ithaca, New York 14850, United States. Email: <a href="mailto:hda1@cornell.edu">hda1@cornell.edu</a>

#### Professor Raymond E. Schaak

Dept. of Chemistry, Dept. of Chemical Engineering, and Materials Science Institute,104 Chemistry Building, The Pennsylvania State University. Email: <a href="mailto:res20@psu.edu">res20@psu.edu</a>

#### **Author Contributions**

All authors have given approval to the final version of the manuscript.

#### **Funding Sources**

H.D.A, M.J.T, and S.L. would like to acknowledge the DMREF and INFEWS programs of the National Science Foundation under Grant No. DMREF-1729338 as well as the Cornell Energy Systems Institute (CESI), the Energy Materials Center at Cornell (emc2), an Energy Frontier Research Center funded by the U.S. Department of Energy, Office of Science, the Office of Basic Energy Sciences under award number DE-SC0001086.

R.E.S. and C.R.M would like to acknowledge the U.S. National Science Foundation under grant DMR-2210442.

#### Notes

The authors declare no competing interests.

### **ACKNOWLEDGMENT**

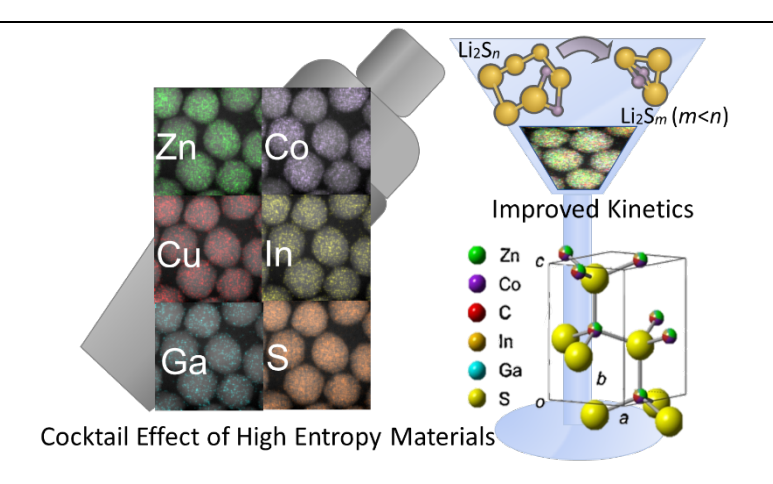
XPS usage was supported by NSF through the Cornell University Materials Research Science and Engineering Center DMR-1719875. TEM imaging and X-ray diffraction were performed at the Materials Characterization Lab of the Penn State Materials Research Institute.

#### **REFERENCES**

- (1) Lang, S.; Feng, X.; Seok, J.; Yang, Y.; Krumov, M. R.; Molina Villarino, A.; Lowe, M. A.; Yu, S. H.; Abruña, H. D. Lithium–Sulfur Redox: Challenges and Opportunities. *Curr Opin Electrochem* **2021**, *25*, 100652. https://doi.org/10.1016/J.COELEC.2020.100652.
- (2) Zheng, D.; Wang, G.; Liu, D.; Si, J.; Ding, T.; Qu, D.; Yang, X.; Qu, D. The Progress of Li–S Batteries—Understanding of the Sulfur Redox Mechanism: Dissolved Polysulfide Ions in the Electrolytes. *Adv Mater Technol* **2018**, *3* (9), 1700233. https://doi.org/10.1002/ADMT.201700233.
- (3) Park, C.; Ronneburg, A.; Risse, S.; Ballauff, M.; Kanduč, M.; Dzubiella, J. Structural and Transport Properties of Li/S Battery Electrolytes: Role of the Polysulfide Species. *Journal of Physical Chemistry C* **2019**, *123* (16), 10167–10177. https://doi.org/10.1021/ACS.JPCC.8B10175/SUPPL\_FILE/JP8B1 0175 SI 001.PDF.
- (4) Manthiram, A.; Fu, Y.; Chung, S. H.; Zu, C.; Su, Y. S. Rechargeable Lithium-Sulfur Batteries. *Chem Rev* **2014**, *114* (23), 11751–11787.
- $\label{lem:https://doi.org/10.1021/CR500062V/SUPPL_FILE/CR500062V\_SI\_001.PDF.$
- (5) Kim, S. J.; Kim, K.; Park, J.; Sung, Y. E. Role and Potential of Metal Sulfide Catalysts in Lithium-Sulfur Battery Applications. *ChemCatChem* **2019**, *11* (10), 2373–2387. https://doi.org/10.1002/CCTC.201900184.
- (6) Wang, P.; Xi, B.; Huang, M.; Chen, W.; Feng, J.; Xiong, S.; Wang, P.; Xi, B. J.; Huang, M.; Xiong, S. L.; Chen, W. H.; Feng, K. Emerging Catalysts to Promote Kinetics of Lithium–Sulfur Batteries. *Adv Energy Mater* **2021**, *11* (7), 2002893. https://doi.org/10.1002/AENM.202002893.
- (7) Geng, C.; Hua, W.; Wang, D.; Ling, G.; Zhang, C.; Yang, Q.-H. Demystifying the Catalysis in Lithium–Sulfur Batteries: Characterization Methods and Techniques. *SusMat* **2021**, *1* (1), 51–65. https://doi.org/10.1002/SUS2.5.
- (8) Zhang, N.; Yang, Y.; Feng, X.; Yu, S.-H.; Seok, J.; Muller, D.; Abruña, H., Sulfur Encapsulation by MOF-Derived CoS2 Embedded in Carbon Hosts for High-Performance Li-S Batteries. J. Mater. Chem. A 2019, 7 (39), 21128-21139. https://doi.org/10.1039/C9TA06947J
- (9) Shen, Z.; Jin, X.; Tian, J.; Li, M.; Yuan, Y.; Zhang, S.; Fang, S.; Fan, X.; Xu, W.; Lu, H.; Lu, J.; Zhang, H. Cation-Doped ZnS Catalysts for Polysulfide Conversion in Lithium–Sulfur Batteries. *Nature Catalysis* 2022 5:6 2022, 5 (6), 555–563. https://doi.org/10.1038/s41929-022-00804-4.
- (10) Dong, Y.; Cai, D.; Li, T.; Yang, S.; Zhou, X.; Ge, Y.; Tang, H.; Nie, H.; Yang, Z. Sulfur Reduction Catalyst Design Inspired by Elemental Periodic Expansion Concept for Lithium-Sulfur Batteries. *ACS Nano* **2022**, *16* (4), 6414–6425. https://doi.org/10.1021/ACSNANO.2C00515/ASSET/IMAGES/L ARGE/NN2C00515 0006.JPEG.
- (11) McCormick, C. R.; Schaak, R. E. Simultaneous Multication Exchange Pathway to High-Entropy Metal Sulfide Nanoparticles. *J Am Chem Soc* **2021**, *143* (2), 1017–1023. https://doi.org/10.1021/JACS.0C11384/ASSET/IMAGES/LARGE/JA0C11384\_0006.JPEG.
- (12) Wu, D.; Kusada, K.; Yamamoto, T.; Toriyama, T.; Matsumura, S.; Kawaguchi, S.; Kubota, Y.; Kitagawa, H. Platinum-Group-Metal High-Entropy-Alloy Nanoparticles. *J Am Chem Soc* **2020**, *142* (32), 13833–13838.

- https://doi.org/10.1021/JACS.0C04807/ASSET/IMAGES/LARGE/JA0C04807\_0004.JPEG.
- (13) Rost, C. M.; Sachet, E.; Borman, T.; Moballegh, A.; Dickey, E. C.; Hou, D.; Jones, J. L.; Curtarolo, S.; Maria, J. P. Entropy-Stabilized Oxides. *Nature Communications 2015 6:1* **2015**, *6* (1), 1–8. https://doi.org/10.1038/ncomms9485.
- (14) Li, K.; Chen, W. Recent Progress in High-Entropy Alloys for Catalysts: Synthesis, Applications, and Prospects. *Mater Today Energy* **2021**, *20*, 100638. https://doi.org/10.1016/J.MTENER.2021.100638.
- (15) Li, H.; Lai, J.; Li, Z.; Wang, L. Multi-Sites Electrocatalysis in High-Entropy Alloys. *Adv Funct Mater* **2021**, *31* (47), 2106715. https://doi.org/10.1002/ADFM.202106715.
- (16) Xin, Y.; Li, S.; Qian, Y.; Zhu, W.; Yuan, H.; Jiang, P.; Guo, R.; Wang, L. High-Entropy Alloys as a Platform for Catalysis: Progress, Challenges, and Opportunities. *ACS Catal* **2020**, *10* (19), 11280–11306.
- $\label{eq:https://doi.org/10.1021/ACSCATAL.0C03617/ASSET/IMAGES/LARGE/CS0C03617\_0015.JPEG.$
- (17) Kumar Katiyar, N.; Biswas, K.; Yeh, J.-W.; Sharma, S.; Sekhar Tiwary, C. A Perspective on the Catalysis Using the High Entropy Alloys. *Nano Energy* **2021**, *88*, 106261. https://doi.org/10.1016/J.NANOEN.2021.106261.
- (18) George, E. P.; Raabe, D.; Ritchie, R. O. High-Entropy Alloys. *Nature Reviews Materials 2019 4:8* **2019**, *4* (8), 515–534. https://doi.org/10.1038/s41578-019-0121-4.
- (19) de Trizio, L.; Manna, L. Forging Colloidal Nanostructures via Cation Exchange Reactions. *Chem Rev* **2016**, *116* (18), 10852–10887. https://doi.org/10.1021/acs.chemrev.5b00739.
- (20) Bard, A. J.; Faulkner, L. R. *Electrochemical Methods: Fundamentals and Applications.*
- (21) Finkelstein, D. A.; Da Mota, N.; Cohen, J. L.; Abruña, H. D. Rotating Disk Electrode (RDE) Investigation of BH4- and BH3OH-Electro-Oxidation at Pt and Au: Implications for BH 4- Fuel Cells. *Journal of Physical Chemistry C* **2009**, *113* (45), 19700–19712. https://doi.org/10.1021/JP900933C/SUPPL\_FILE/JP900933C\_SI\_001.PDF.
- (22) Finkelstein, D. A.; Kirtland, J. D.; Mota, N. Da; Stroock, A. D.; Abruña, H. D. Alternative Oxidants for High-Power Fuel Cells Studied by Rotating Disk Electrode (RDE) Voltammetry at Pt, Au, and Glassy Carbon Electrodes. *Journal of Physical Chemistry C* **2011**, 115 (13), 6073–6084. https://doi.org/10.1021/JP1082505/ASSET/IMAGES/JP-2010-082505\_M031.GIF.
- (23) Finkelstein, D. A.; Jones, D. J.; Hernandez-Burgos, K.; Abruña, H. D. Electro-Oxidation of BH4– in Dimethylsulfoxide and Dimethylformamide Studied by Rotating Disk Electrode Voltammetry. *J Power Sources* **2011**, *196* (15), 6223–6227. https://doi.org/10.1016/J.JPOWSOUR.2011.03.034.
- (24) Zoski, C. G. Handbook of Electrochemistry. *Handbook of Electrochemistry* **2007**, 1–892. https://doi.org/10.1016/B978-0-444-51958-0.X5000-9.
- (25) Theibault, M. J.; Chandler, C.; Dabo, I.; Abruña, H. D. Transition Metal Dichalcogenides as Effective Catalysts for High-Rate Lithium-Sulfur Batteries. *ACS Catal* **2023**, *13*, 3684–3691. https://doi.org/10.1021/ACSCATAL.3C00186/ASSET/IMAGES/L ARGE/CS3C00186\_0010.JPEG.
- (26) Wang, L.; Zhang, L.; Lu, X.; Wu, F.; Sun, X.; Zhao, H.; Li, Q. Surprising Cocktail Effect in High Entropy Alloys on Catalyzing Magnesium Hydride for Solid-State Hydrogen Storage. *Chemical Engineering Journal* **2023**, 465, 142766. https://doi.org/10.1016/J.CEJ.2023.142766.
- (27) Katzbaer, R. R.; dos Santos Vieira, F. M.; Dabo, I.; Mao, Z.; Schaak, R. E. Band Gap Narrowing in a High-Entropy Spinel Oxide Semiconductor for Enhanced Oxygen Evolution Catalysis. *J Am*

- *Chem Soc* **2023**, 145, 40. https://doi.org/10.1021/JACS.2C12887/ASSET/IMAGES/LARGE /JA2C12887\_0007.JPEG.
- (28) Lang, S.; Colletta, M.; Krumov, M. R.; Seok, J.; Kourkoutis, L. F.; Wen, R.; Abruña, H. D. Multidimensional Visualization of the Dynamic Evolution of Li Metal via in Situ/Operando Methods. *Proc Natl Acad Sci U S A* **2023**, *120* (7), e2220419120. https://doi.org/10.1073/PNAS.2220419120/SUPPL FILE/PNAS. 2220419120.SM02.MP4.
- (29) Cui, M.; Yang, C.; Li, B.; Dong, Q.; Wu, M.; Hwang, S.; Xie, H.; Wang, X.; Wang, G.; Hu, L.; Cui, M.; Yang, C.; Dong, Q.; Wu, M.; Xie, H.; Wang, X.; Hu, L.; Li, B.; Wang, G.; Hwang, S. High-Entropy Metal Sulfide Nanoparticles Promise High-Performance Oxygen Evolution Reaction. *Adv Energy Mater* **2021**, *11* (3), 2002887. https://doi.org/10.1002/AENM.202002887.
- (30) Shen, B.; Huang, L.; Shen, J.; Hu, X.; Zhong, P.; Zheng, C. Y.; Wolverton, C.; Mirkin, C. A. Morphology Engineering in Multicomponent Hollow Metal Chalcogenide Nanoparticles. *ACS Nano* **2023**, *17* (5), 4642–4649. https://doi.org/10.1021/ACSNANO.2C10667/ASSET/IMAGES/L ARGE/NN2C10667\_0005.JPEG.
- (31) Lang, S.; Yu, S. H.; Feng, X.; Krumov, M. R.; Abruña, H. D. Understanding the Lithium–Sulfur Battery Redox Reactions via Operando Confocal Raman Microscopy. *Nature Communications 2022* 13:1 2022, 13 (1), 1–11. https://doi.org/10.1038/s41467-022-32139-w.



Insert Table of Contents artwork here